Interaction of *rac*-[Ru(5,6-dmp)$_3$]$^{2+}$ with DNA: Enantiospecific DNA Binding and Ligand-Promoted Exciton Coupling

Palanisamy Uma Maheswari, Venugopal Rajendiran, Helen Stoeckli-Evans, and Mallayan Palaniandavar*

School of Chemistry, Bharathidasan University, Tiruchirappalli-620 024, India, and Department of Chemistry, University of Neuchatel, CH-2007 Neuchatel, Switzerland

Received June 10, 2005

The X-ray crystal structure of the complex *rac*-[Ru(5,6-dmp)$_3$]Cl$_2$ (5,6-dmp = 5,6-dimethyl-1,10-phenanthroline) reveals a distorted octahedral coordination geometry with the Ru–N bond distances shorter than in its phen analogue. Absorption spectral titrations with CT DNA reveal that *rac*-[Ru(5,6-dmp)$_3$]$^{2+}$ interacts (K_b, $(8.0 \pm 0.2) \times 10^4$ M^{-1}) much more strongly than its phen analogue. The emission intensity of the 5,6-dmp complex is dramatically enhanced on binding to DNA, which is higher than that of the phen analogue. Also, interestingly, time-resolved emission measurements on the DNA-bound complex shows biexponential decay of the excited states with the lifetimes of short- and long-lived components being higher than those for the phen analogue. The CD spectral studies of *rac*-[Ru(5,6-dmp)$_3$]$^{2+}$ bound to CT DNA provide a definite and elegant evidence for the enantiospecific interaction of the complex with B-form DNA. Competitive DNA binding studies using *rac*-[Ru(phen)$_3$]$^{2+}$ provide support for the strong binding of the complex with DNA. The Δ-enantiomer of *rac*-[Ru(5,6-dmp)$_3$]$^{2+}$ binds specifically to the right-handed B-form of poly d(GC)$_{12}$ at lower ionic strength (0.05 M NaCl), and the Λ-enantiomer binds specifically to the left-handed Z-form of poly d(GC)$_{12}$ generated by treating the B-form with 5 M NaCl. The strong electronic coupling of the DNA-bound complex with the unbound complex facilitates the change in its enantiospecificity upon changing the conformation of DNA. The ^{1}H NMR spectra of *rac*-[Ru(5,6-dmp)$_3$]$^{2+}$ bound to poly d(GC)$_{12}$ reveal that the complex closely interacts most possibly in the major grooves of DNA. Electrochemical studies using ITO electrode show that the 5,6-dmp complex stabilizes CT DNA from electrocatalytic oxidation of its guanine base more than the phen analogue does.

Introduction

The study of the nature and dynamics of binding of small molecules to polymeric DNA represents a field of active investigation over the past two decades.[1] The aim of the study has been manifold the design of site- or conformation-specific probes for recognizing the biopolymer structure and the development of selective DNA cleaving agents for mapping or foot printing experiments as well as a more rational drug design.[2,3] The positively charged transition metal (e.g. Pt, Ru, Rh, Co, Zn) complexes with polypyridyl ligands,[4−7] which display intense metal-to-ligand charge transfer (MLCT) absorptions and strong luminescence in the visible region, have the potential to be used as excellent probes of various microenvironments. The study of kinetically inert octahedral Ru(II) complexes as chiral probes for DNA has elicited intense investigation in recent years. The utility of a chiral probe for DNA handedness is limited not only by the sensitivity with which the DNA binding may be detected but also by the sensitivity with which the probe may distinguish the enantiomers.[8] The enantiospecific interaction

* To whom correspondence should be addressed. E-mail: palanim51@yahoo.com.

(1) Pyle, A. M.; Barton, J. K. In *Progress in Inorganic Chemistry*: *Bioinorganic Chemistry*; Lippard, S. J., Ed.; John Wiley & Sons: New York, 1990; Vol. 38, p 413.
(2) Erkkila, K. E.; Odom, D. T.; Barton, J. K. *Chem. Rev.* **1999**, *99*, 2777.
(3) Lerman, L. S. *J. Mol. Biol*. **1961**, *3*, 18.
(4) Jennette, K. W.; Lippard, S. J.; Vassiliades, G. A.; Baner, W. R. *Proc. Natl. Acad. Sci. U.S.A.* **1974**, *71*, 3839.
(5) Komeda, S.; Lutz, M.; Spek, A. L.; Chikuma, M.; Reedijk, J. *Inorg. Chem.* **2000**, *39*, 4230.
(6) Barton, J. K. *Science* **1986**, *233*, 727.
(7) (a) Friedman, A. E.; Chambron, J. C.; Sauvage, J. P.; Turro, N. J.; Barton, J. K. *J. Am. Chem. Soc*. **1990**, *112*, 4960. (b) Bradely, P. M.; Angeles-Boza, A. M.; Dunbar, K. R.; Turro. C. *Inorg. Chem.* **2004**, *43*, 2450. (c) Angeles-Boza, A. M.; Bradely, P. M.; Fu, P. K.-L.; Wicke, S. E.; Bacsa, J.; Dunbar, K. R.; Turro, C. *Inorg. Chem.* **2004**, *43*, 8510.

of the Δ- rather than Λ-enantiomer of *rac*-$[Ru(phen)_3]^{2+}$ (phen = 1,10-phenanthroline) with the right-handed DNA duplex has been an intensive controversial debate.[9−16] In our laboratory we have shown that the peak currents of Δ- rather than Λ-$[Ru(phen)_3]^{2+}$ enantiomers are decreased selectively on binding to CT DNA revealing enantiospecific DNA binding of the Δ-enantiomer to B-DNA.[17] The complex $[Ru(4,7\text{-dip})_3]^{2+}$ (4,7-dip = 4,7-diphenyl-1,10-phenanthroline) leads to stronger enantiospecificity toward B-DNA with Δ-form binding strongly to right-handed B-DNA while both the enantiomers bind to the left-handed Z-DNA equally well.[18] Very recently the DNA binding of variously methyl-substituted $(phen)_3Ru^{II}$ complexes has been investigated, and evidence for the dependence of DNA binding mode on concentration of the ruthenium complex has been obtained.[19] Among the enantiomers of $[Ru(tmp)_3]^{2+}$ (tmp = 3,4,7,8-tetramethyl-1,10-phenanthroline)[20] the Λ-form binds more strongly than the Δ-form and is a specific probe for A-DNA. And in recent years the binding of the Δ-enantiomer of the "molecular light switches" $[Ru(phen)_2(dppz)]^{2+}$ and $[Rh(phen)_2(phi)]^{3+}$ to B-DNA has been clearly proved by ^1H NMR, circular dichroism, linear dichroism, and fluorescence spectral studies.[7,21]

From our laboratory we have reported that incorporation of 5,6 methyl groups on phen ring as in $[Ru(NH_3)_4(5,6\text{-dmp})]^{2+}$ (5,6-dmp = 5,6-dimethyl-1,10-phenanthroline) enhances the hydrophobic interaction of the complex with DNA.[22,23] In fact, among the various methyl-substituted and unsubstituted *N*-methyl-1,10-phenanthrolinium cations the 5,6-dimethyl-substituted *N*-methylphenanthrolinium ion shows the highest DNA binding affinity.[24] Again, through a DNA-fiber EPR study of the ternary copper(II) complexes of amino acids and various phenanthrolines, it has been found that 5,6-dimethyl substitution on the phen ring promotes intercalative binding of the complexes to DNA.[25] Further, in our laboratory $[Cu(5,6\text{-dmp})_2]^{2+}$ has been found to induce an irreversible B to Z conformational change.[26] In addition, $[Os(5,6\text{-dmp})_3]^{2+}$ is reported to have a very high DNA binding affinity and also acts as a DNA sensor and hybridization indicator.[27] In the present investigation we have probed in detail the effect of incorporating 5,6-dimethyl groups on the phen ring on the extent and nature of DNA binding and the stereospecific interaction of *rac*-$[Ru(5,6\text{-dmp})_3]^{2+}$ (Figure 1) with CT DNA and selected synthetic polynucleotides by using absorption, emission, circular dichroism (CD), and ^1H NMR spectral and molecular modeling studies. CD spectral studies reveal that the Δ-form of *rac*-$[Ru(5,6\text{-dmp})_3]^{2+}$ binds enantiopreferentially to the B-form of poly $d(GC)_{12}$ at lower ionic strength (0.05 M NaCl) while the Λ-form binds to the Z-form of poly $d(GC)_{12}$ generated from the B form at higher ionic strength (5 M NaCl). This is interesting as earlier studies[19] have shown that the complex does not bind to DNA at all.

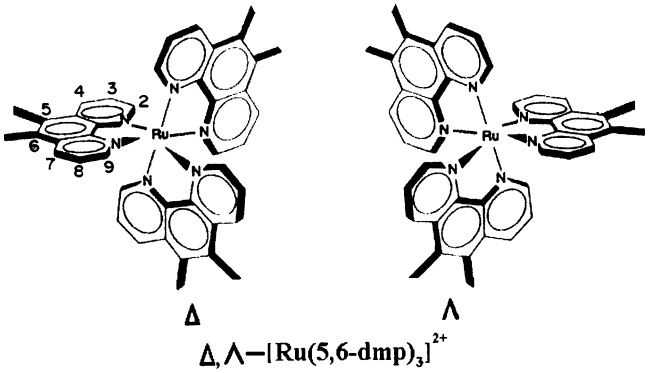

Figure 1. Schematic view of Δ- and Λ-$[Ru(5,6\text{-dmp})_3]^{2+}$.

Results and Discussion

Description of the Structure of *rac*-$Ru(5,6\text{-dmp})_3]Cl_2\cdot 13H_2O$. The X-ray crystal structure of the complex consists of both the Δ- and Λ-enantiomers of monomeric ruthenium(II) complex cation, and the molecular structure of the complex cation with crystallographic atom numbering scheme is illustrated in PLATON drawings (Figure 2A,B). The coordination geometry of the RuN_6 chromophore is distorted from a regular octahedral as a consequence of the small bite angles of the 5,6-dmp ligands (79.18, 79.39, 79.50°), which deviate very much from the ideal angle of 90°. Also, the average bite angle is less than that for the phen analogues $[Ru(phen)_3](PF_6)_2$ (79.8°)[28] and $[Ru(phen)_3](ClO_4)_2$ (80.0°).[29] The 5,6-dmp ligands make an angle of 79.35° with each other, which is a consequence of crystal packing. Interestingly, the average Ru−N bond distance (2.059 Å) is shorter than (Tables 1and 2) those observed for the phen analogues (PF_6^-, 2.063 Å, ClO_4^-, 2.064 Å)[29] indicating that the electron-releasing 5,6-dimethyl groups render the Ru−N bonds stronger.

(8) Barton, J. K.; Basile, L. A.; Danishefshy, A.; Alexandresea, A. *Proc. Natl. Acad. Sci. U.S.A.* **1984**, *81*, 1961.
(9) Ji, L. N.; Zon, X. H.; Ziu, J. G. *Coord. Chem. Rev.* **2001**, *216−217*, 513.
(10) Satyanarayana, S., Dabrowiak, J. C.; Chaires, J. B. *Biochemistry* **1992**, *31*, 9319.
(11) Naing, K.; Takahashi, M.; Taniguchi, M.; Yamagishi, A. *J. Chem. Soc., Chem. Commun.* **1993**, 402.
(12) Barton, J. K.; Danishefsky, A. T.; Goldberg, J. M. *J. Am. Chem. Soc*. **1984**, *106*, 2172.
(13) Rehmann, J. P.; Barton, J. K. *Biochemistry* **1990**, *29*, 1710.
(14) Eriksson, M.; Leijon, M.; Hiort, C.; Norden, B.; Graslund, A. *J. Am. Chem. Soc*. **1992**, *114*, 4933.
(15) Satyanarayana, S.; Dabrowiak, J. C.; Chaires, J. B. *Biochemistry* **1993**, *32*, 2573.
(16) Carter, M. T.; Bard, A. J. *J. Am. Chem. Soc*. **1987**, *109*, 7528.
(17) Mahadevan, S.; Palaniandavar, M. *Bioconjugate Chem.* **1996**, *7*, 138.
(18) Kumar, C. V.; Barton, J. K.; Turro, N. J. *J. Am. Chem. Soc*. **1985**, *107*, 5518.
(19) Coggan, D. Z. M.; Haworth I. S.; Bates, P. J.; Robinson, A.; Rodger, A. *Inorg. Chem.* **1999**, *38*, 4486-4497.
(20) Mei, H. J.; Barton, J. K. *Proc. Natl. Acad. Sci. U.S.A.* **1988**, *85*, 1339. Biochemistry.
(21) Collins, J. G.; Shields, T. P.; Barton, J. K. *J. Am. Chem. Soc.* **1994**, *116*, 9840.
(22) Uma Maheswari, P.; Palaniandavar, M. *Inorg. Chim. Acta* **2004**, *357*, 901.
(23) Uma Maheswari, P.; Palaniandavar, M. Unpublished results.
(24) Gabbay, E. J.; Scofield, R. E.; Baxter, C. S. *J. Am. Chem. Soc*. **1973**, *95*, 7850.
(25) Chikira, M.; Tomizawa, Y.; Fukita, D.; Sugizaki, T.; Sugawara, N.; Yamazaki, T.; Sasano, A.; Shindo, H.; Palaniandavar, M.; Antholine, W. E. *J. Inorg. Biochem.* **2002**, *89*, 163.
(26) Mahadevan, S.; Palaniandavar, M. *Inorg. Chem*. **1998**, *37*, 3927.
(27) Maruyama, K.; Motonaka, J.; Mishima, Y.; Matsuzaki, Y.; Nakabayashi, I.; Nakabayashi, Y. *Sens. Actuators, B* **2001**, *76*, 215.
(28) J. Breu, A. J. Stoll, *Acta Crystallogr*. **1996**, *C52*, 1174.
(29) Wu, J. Z.; Zhou, Z. Y.; Ji, L. N. *Cryst. Res. Technol*. **2001**, *1*, 101.

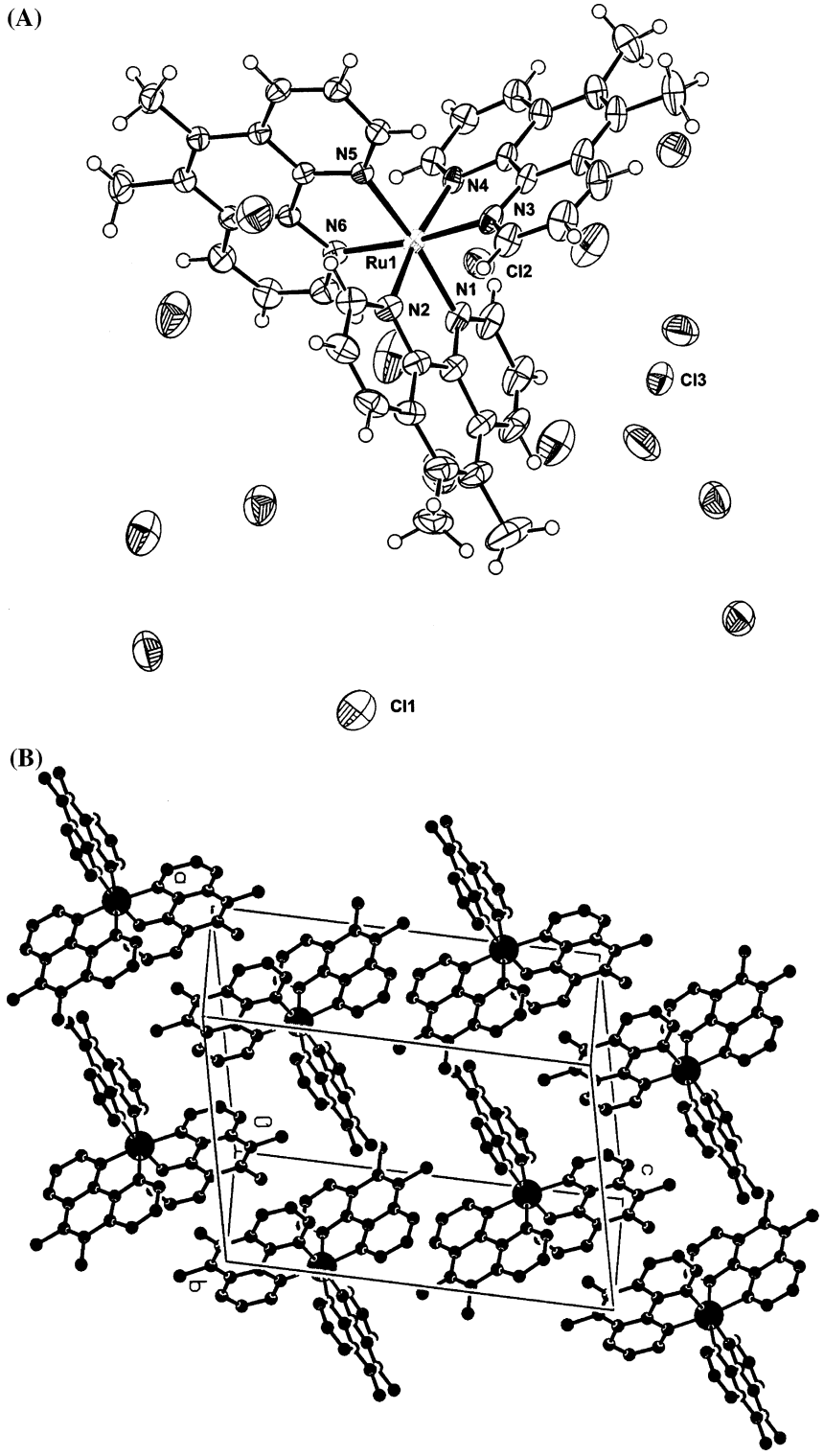

Figure 2. (A) Representation of the X-ray crystal structure of RuN6, with all non-hydrogen atoms shown as 50% thermal ellipsoids. (B) Unit cell packing diagram of *rac*-[Ru(5,6-dmp)$_3$]Cl$_2$ showing both the Δ- and Λ-enantiomers of the monomeric ruthenium(II) complex cation. (Lattice water and the chloride anion are removed for clarity.)

Absorption Spectral Studies. The complex *rac*-[Ru(5,6-dmp)$_3$]$^{2+}$ exhibits an intense metal to ligand charge transfer (MLCT) band at 455 nm with a shoulder around 430 nm. On titration of a solution of the complex (4.0×10^{-5} M) with CT DNA (R = [DNA]/[Ru complex] = 0−40), a large decrease in intensity with no red-shift is observed in the main feature (Figure 3A). The pronounced hypochromism observed (Δε, 40% at R = 40) is higher than that (Δε, 12%, red-shift 2 nm) for the analogous *rac*-[Ru(phen)$_3$]$^{2+}$.[12,30] From the observed spectral changes, the value of the intrinsic equilibrium DNA binding constant K_b was determined by regression analysis using the Bard and Carter equation[31]

(30) Pyle, A. M.; Rehmann, J. P.; Meshoyer, R.; Kumar, C. V.; Turro, N. J.; Barton, J. K. *J. Am. Chem. Soc.* **1989**, *111*, 3051.

Table 1. Summary of Crystal Data and Refinement Parameters for *rac*-$[Ru(5,6\text{-dmp})_3]^{2+}$

empirical formula	$C_{42}H_{62}Cl_2N_6O_{13}Ru$
	$[C_{42}H_{36}N_6Ru]^{2+}(Cl^-)_2 \cdot 13H_2O$
fw	1030.95
temp	173(2) K
wavelength	0.710 73 Å
cryst system	triclinic
space group	$P\bar{1}$
unit cell dimens	$a = 11.7020(10)$ Å, $\alpha = 103.159(6)°$
	$b = 12.2803(9)$ Å, $\beta = 105.697(6)°$
	$c = 18.7338(14)$ Å, $\gamma = 100.053(6)°$
V, Z	2442.3(3) Å^3, 2
D(calcd)	1.402 g/cm^3
linear abs coeff	0.496 mm^{-1}
F(000)	1076
cryst size	0.50 × 0.50 × 0.50 mm
reflcns measd	29 183
indpndt reflcns	13 041 (R(int) = 0.0498)
obsd reflcns	10 933
θ range for data collcn	1.86−29.33°
index ranges	$-16 \le h \le 15$, $-16 \le k \le 16$, $-25 \le l \le 24$
refinement method	full-matrix least-squares on F^2
goodness-of-fit on F^2	1.160
final R indices [$I > 2\sigma(I)$]	R1 = 0.0703,[a] wR2 = 0.1790[b]
R indices (all data)	R1 = 0.0855,[a] wR2 = 0.1869[b]

[a] $R = \sum||F_o| - |F_c||/\sum|F_o|$. [b] $R = \{\sum w[(F_o^2 - F_c^2)^2/\sum w[(F_o^2)^2]\}^{1/2}$.

Table 2. Selected Bond Lengths (Å) and Angles (deg) for *rac*-$[Ru(5,6\text{-dmp})_3]^{2+}$

Ru(1)−N(2)	2.054(4)	Ru(1)−N(4)	2.057(4)
Ru(1)−N(5)	2.058(3)	Ru(1)−N(6)	2.060(4)
Ru(1)−N(3)	2.061(4)	Ru(1)−N(1)	2.065(4)
N(2)−Ru(1)−N(4)	171.09(14)	N(2)−Ru(1)−N(5)	95.11(14)
N(4)−Ru(1)−N(5)	91.02(13)	N(2)−Ru(1)−N(6)	90.65(14)
N(4)−Ru(1)−N(6)	96.83(14)	N(5)−Ru(1)−N(6)	79.50(13)
N(2)−Ru(1)−N(3)	93.59(15)	N(4)−Ru(1)−N(3)	79.39(15)
N(5)−Ru(1)−N(3)	95.10(14)	N(6)−Ru(1)−N(3)	173.42(15)
N(2)−Ru(1)−N(1)	79.18(15)	N(4)−Ru(1)−N(1)	95.11(15)
N(5)−Ru(1)−N(1)	173.06(15)	N(6)−Ru(1)−N(1)	96.52(14)
N(3)−Ru(1)−N(1)	89.23(14)		

(Figure 3B, K_b, 8.0 ± 0.2 × 10^4 M^{-1}; s, 1.5 base pairs), which is higher than that for *rac*-$[Ru(phen)_3]^{2+}$ (K_b, 6.2 ± 0.2 × 10^3 M^{-1}; s, 4 base pairs) under identical conditions. Interesting changes are observed also in the $\pi \rightarrow \pi^*$ bands (270, 242 nm) of the complex on adding DNA: hypochromism (30%) up to an R value of 0.5 and then a strong increase in absorbance until an R value of 2.5 revealing aggregation of the complex in the presence of DNA. The higher DNA binding affinity of the 5,6-dmp complex is interesting because the 5,6-dimethyl groups would be expected to hinder the partial insertion of the phen ring into the DNA base pairs. It appears that the size and shape of the complex is tuned to closely fit into the helical groove leading to a stronger hydrophobic interaction of the 5,6-dimethyl groups with DNA surface (cf. below).[30,32] A similar enhanced hydrophobic interaction of $[Ru(NH_3)_4(5,6\text{-dmp})]^{2+}$ [22] and $[Ru(5,6\text{-dmp})_2(dppz)]^{2+}$ [23] complexes with CT DNA has been observed by us previously.

Emission Spectral Studies. In aqueous tris-buffer solution the 5,6-dmp complex shows a strong emission at 590 nm when excited at the λ_{max} of 455 nm (Table 3). On treatment of the complex with CT DNA (R = 10 = [DNA]/[Ru complex]) the emission is enhanced dramatically ($I/I_0 = 2.82$, where I_0 and I are the emission intensities in the absence and presence of CT DNA, Figure 4A). Interestingly, this enhancement in emission is higher than that observed for *rac*-$[Ru(phen)_3]^{2+}$ under identical conditions (I/I_0, 2.20, Figure 4B). Also, a small blue-shift (2 nm) in the emission maximum is observed for the DNA-bound 5,6-dmp complex in contrast to the red shift of 11 nm for the phen analogue.[12] It is suggested that the 5,6-dmp complex interacts on the hydrophobic DNA environment with a solvent accessibility lower than that for the phen analogue.[33] Further, the ferrocyanide quenching patterns determined for both the DNA-bound 5,6-dmp and phen complexes in the steady state are not linear (Figure S1). Interestingly, the Stern−Volmer constant obtained for the 5,6-dmp complex is lower than that for the phen complex (K_{SV}: 5,6-dmp, 94; phen, 422 M^{-1}; Table 3). This reveals that the 5,6-dmp complex species are protected from the quencher more than the phen complex,

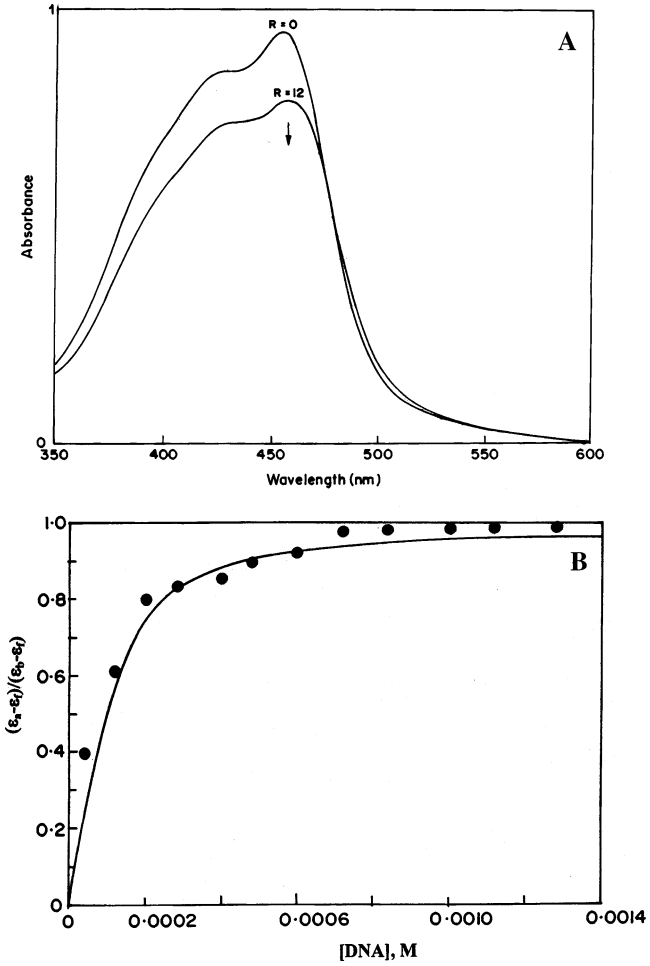

Figure 3. (A) Absorption spectra of *rac*-$[Ru(5,6\text{-dmp})_3]^{2+}$ (4 × 10^{-5} M) in 5 mM Tris HCl buffer at pH 7.2, in the absence (R = 0) and presence (R = 12) of increasing amounts of DNA. (B) Plot of $(\epsilon_a - \epsilon_f)/(\epsilon_b - \epsilon_f)$ vs [DNA] for *rac*-$[Ru(5,6\text{-dmp})_3]^{2+}$. The best fit line, superimposed on the data, according to the equation yields $K_b = (8.0 \pm 0.2) \times 10^4$ M^{-1} (s = 1.5).

(31) Carter, M. T.; Rodriguez, M.; Bard, A. J. *J. Am. Chem. Soc.* **1989**, *111*, 8901.
(32) Barton, J. K.; Goldberg, J. M.; Kumar, C. V.; Turro, N. J. *J. Am. Chem. Soc.* **1986**, *108*, 2081.
(33) Turro, C.; Bossman, S. H.; Jenkins, Y.; Barton, J. K.; Turro, N. J. *J. Am. Chem. Soc.* **1995**, *117*, 9026.

Table 3. Luminescence Properties of the Ruthenium Complexes in the Absence and Presence of CT DNA at 25 °C

complex	λ_{excit}[a] (nm)	λ_{emis}[b] $R=0$	λ_{emis}[b] $R=40$	Int[c]	I/I_0[d]	K_{sv}[e] (M^{-1}) (steady state)	τ (ns)	τ_o[f] (ns) sh	τ_o[f] (ns) lg	K_{sv}[g] (M^{-1}) sh	K_{sv}[g] (M^{-1}) lg	$10^{-7}k_q$[h] (M^{-1} s^{-1}) sh	$10^{-7}k_q$[h] (M^{-1} s^{-1}) lg	P[i] $R=0$	P[i] $R=40$
$[Ru(5,6\text{-dmp})_3)]^{2+}$	455	590	588	1.90	3.00	94	621	760 (35)	2070 (65)	195	85	25.0	4.1	0.080	0.366
$[Ru(phen)_3]^{2+}$	452	582	592	1.50	2.33	422	528	560 (37)	1750 (63)	363	61	65.0	3.5	0.012	0.311

[a] Excitation wavelength maximum of the complexes. [b] Emission wavelength maximum of the complexes in the presence and absence of CT DNA. [c] Emission intensity of the complexes relative to $[Ru(bipy)_3]^{2+}$. [d] Ratio of the emission intensity of the complexes in the presence (I) to that in the absence (I_0) of CT DNA at $R = 40$. [e] Stern−Volmer constants ([Q] > 0.4 mM) for the quenching of the complexes by $[Fe(CN)_6]^{4-}$ in the presence of DNA (steady-state emission). The value for $[Ru(phen)_3]^{2+}$ is consistent with the reported value.[32] [f] Lifetimes obtained for the complexes by convolution of biexponential decay in the presence of DNA ($R = 40$) (fraction of the species provided in parentheses). [g] Stern−Volmer constants ([Q] > 0.4 mM) for $[Fe(CN)_6]^{4-}$ quenching of the complexes in the presence of DNA (time-resolved luminescence). [h] Rates calculated for the quenching of the complexes by $[Fe(CN)_6]^{4-}$. [i] Polarization values of the complexes in the absence and presence of CT DNA. Measurements were made at $R = 40$, where R = [DNA]/[Ru complex] and concentration of ruthenium solutions = 1×10^{-5} M.

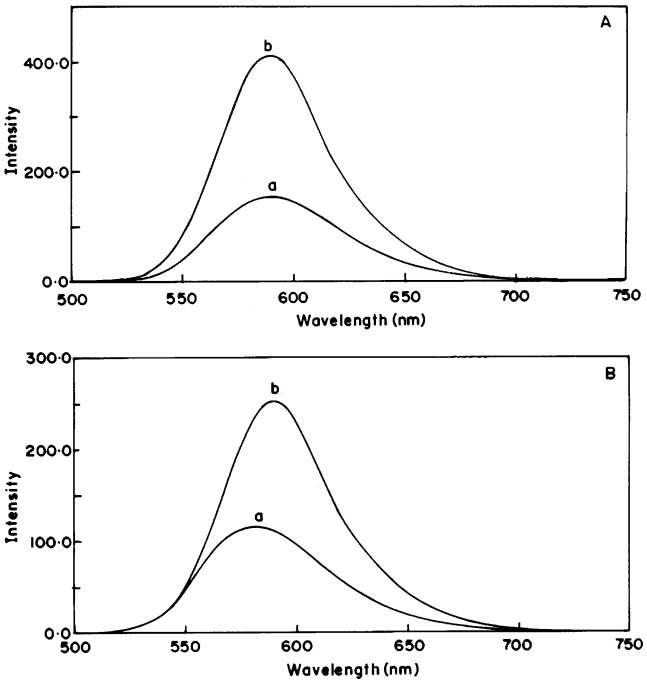

Figure 4. (A) Emission spectra of the *rac*-$[Ru(5,6\text{-dmp})_3]^{2+}$ in the (a) absence and (b) presence of CT DNA at R value of 10 (concentration of CT DNA = 10×10^{-6} M). (B) Emission spectra of the *rac*-$[Ru(phen)_3]^{2+}$ in the (a) absence and (b) presence of CT DNA at R value of 10 (concentration of CT DNA = 10×10^{-6} M).

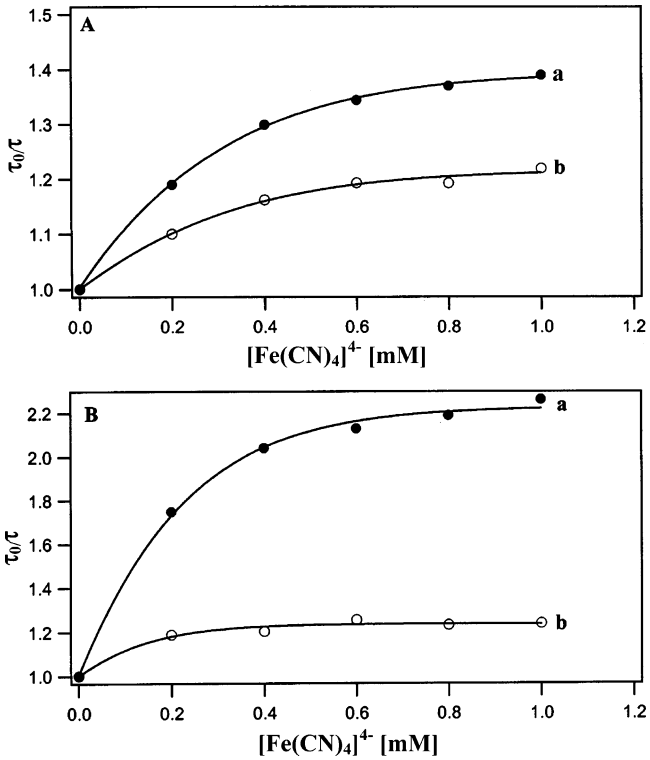

Figure 5. (A) Stern−Volmer plots of *rac*-$[Ru(5,6\text{-dmp})_3]^{2+}$ with short-lived component quenching by $[Fe(CN)_6]^{4-}$ (a) and long-lived component quenching by $[Fe(CN)_6]^{4-}$ (b) at R value of 40 (concentration of CT DNA = 10×10^{-6} M). (B) Stern−Volmer plots of *rac*-$[Ru(phen)_3]^{2+}$ with short-lived component quenching by $[Fe(CN)_6]^{4-}$ (a) and long-lived component quenching by $[Fe(CN)_6]^{4-}$ (b) at R value of 40 (concentration of CT DNA = 10×10^{-6} M).

which is expected of its higher binding affinity (cf above) and larger enhancement in emission.

Time-correlated single photon counting experiments reveal that in the absence of DNA both the 5,6-dmp and phen complexes exhibit strictly monoexponential emission decay. However, in the presence of CT DNA ($R = 40$ = [DNA]/[Ru complex]) both the complexes show biexponential decay profiles typical of short- and long-lived components. For both the complexes the short-lived species would correspond to the unbound species and/or nonspecific ionic association as revealed by their τ_0 values, which are close to the intrinsic lifetimes of the complexes. Also, for both the complexes the lifetimes obtained for the long-lived components are ~3-fold longer than the short-lived species revealing stronger binding of the long-lived species to DNA. Further, the rates of quenching (k_q) by ferrocyanide of the short-lived components of both the complexes are higher than the long-lived species and the ratio of the fraction of the long-lived to short-lived species increases (1.9 to 9.9) with increase in concentration of the quencher (Figure 5A,B). Interestingly, the lifetimes obtained for long-lived species of the 5,6-dmp complex are higher than that for the phen analogue, confirming its stronger DNA binding. Also, for the short-lived species the k_q values of the 5,6-dmp complex are lower than that for the phen complex, as expected. However, for the long-lived species the k_q value of the former is higher than that for the latter suggesting that the long-lived species of the latter is less accessible to ferrocyanide on account of its partial intercalative interaction.

The magnitude of steady-state luminescence polarization P, given by eq 1,

$$P = (I_{||} - I_{\perp})/(I_{||} + I_{\perp}) \quad (1)$$

where $I_{||}$ and $I_{\perp}$ are the emission intensities respectively at parallel and perpendicular directions to the exciting light,

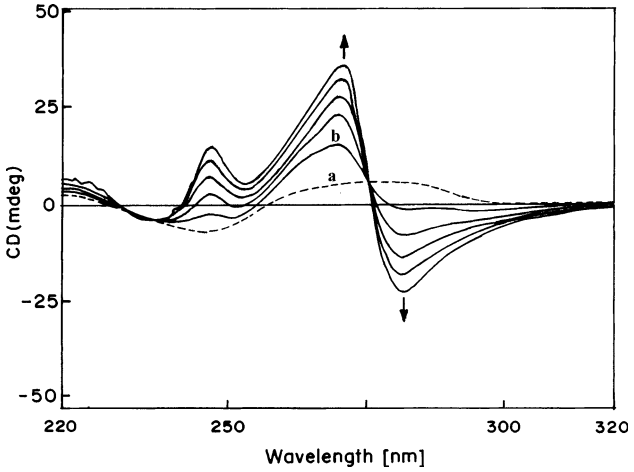

Figure 6. Circular dichroism spectra of CT DNA in the absence (a) and presence (b) of $[Ru(5,6\text{-dmp})_3]^{2+}$ ($1/R = 0-2$) (concentration of CT DNA $= 2 \times 10^{-5}$ M).

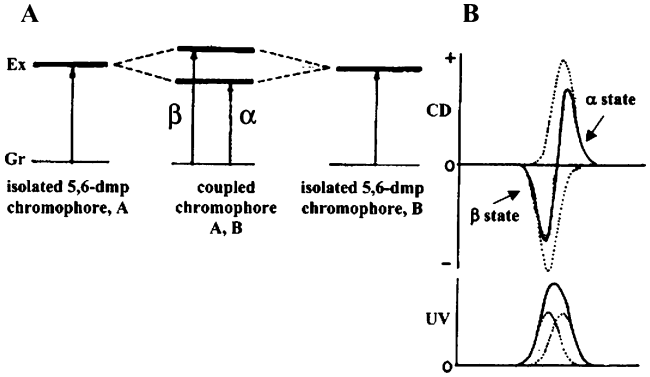

Figure 7. (A) Schematic diagram of exciton coupling of two identical 5,6-dmp chromophores in *rac*-$[Ru(5,6\text{-dmp})_3]^{2+}$ and the splitting of the excited states of the coupled chromophores (bound/unbound complex) into α and β states. (B) CD and UV curves of the individual and exciton coupled chromophores and the resultant induced CD with positive and negative Cotton effects.

may be regarded as a measure of restriction in rotation of excited states of DNA-bound molecules. For the 5,6-dmp and phen complexes the values of *P* have been measured at 25 °C by exciting them at 455 nm and then observing the emission using suitable filters to cut off the exciting light. The very low values of *P* measured for the complexes in the absence of DNA (phen, 0.012; 5,6-dmp, 0.080) reveal that the complexes rotate freely in aqueous solution. The values of *P* measured for 5,6-dmp and phen complexes, when completely bound to CT DNA ($R = 40$), are higher than those in isotropic solution revealing that the complexes become highly oriented upon binding to the biopolymer. Interestingly, the value of *P* for 5,6-dmp complex (0.366) is higher than that (0.311) for the phen analogue, which is consistent with the above absorption and emission spectral results. Thus, the hydrophobic interaction of the 5,6-dimethyl groups with DNA surface leads to more rigid DNA binding of the 5,6-dmp complex.

Circular Dichroic Spectral Studies. On addition of *rac*-$[Ru(5,6\text{-dmp})_3]^{2+}$ complex to CT DNA (2×10^{-5} M, $1/R = 0-2 =$ [Ru complex]/[DNA]), the characteristic bands[34−36] of DNA due to base stacking (275 nm) and that due to right-handed helicity (248 nm) disappear and a biphasic CD signal[37] with positive (270 nm) and negative (280 nm) maxima and a zero cross over at 275 nm are observed. A small negative (240 nm) and a positive signal (248 nm) with a cross over at 245 nm are also observed. Interestingly, the intensities of the biphasic signals are higher than those of the original DNA bands (Figure 6), increase with increase in value of $1/R$, and reach a maximum at $1/R = 2$. Also, the zero cross over observed at 275 nm correspond to the λ_{max} of the $\pi-\pi^*$ transition located on the 5,6-dmp ligand. The CD signal observed is typical of the Δ-form of $[Ru(5,6\text{-dmp})_3]^{2+}$ (Figure S2) and other analogous substituted phen complexes.[38,39] So, it is clear that the Δ-enantiomer of *rac*-$[Ru(5,6\text{-dmp})_3]^{2+}$ binds to CT DNA enantiopreferentially and the biphasic CD signal observed actually corresponds to exciton CD arising from the exciton coupling[40−45] between coordinated 5,6-dmp ligands of DNA-bound and unbound complexes (Figure 7). This type of induced CD signal is not discerned for *rac*-$[Ru(phen)_3]^{2+}$ and analogous complexes of other methyl-substituted phenanthrolines on interaction with DNA (Figure S3). Interestingly, when the concentration of DNA is increased from $R = 1$ to 10 (=[DNA]/[Ru complex]) by keeping the complex concentration constant, inverted CD signals are observed with their intensities increasing with *R* value, reaching a maximum at $R = 3$ and then remaining constant (Figure S4). This suggests the deaggregation of the exciton coupled complex species and then binding to the DNA sites the availability of which increases with increase in concentration of DNA. When the CD response obtained for CT DNA bound to *rac*-$[Ru(5,6\text{-dmp})_3]^{2+}$ ($R = 2$) is monitored over time (0 to 60 min), only slight changes in the positive rather than negative signal are observed (Figure S5). Again, when the signals are monitored as a function of temperature (7−97 °C), surprisingly, no decrease but a slight increase in intensities of both the positive and negative components is observed (Figure S6). This reveals that the double-stranded DNA is strongly stabilized on binding to *rac*-$[Ru(5,6\text{-dmp})_3]^{2+}$ at higher temperatures.

(34) Hiort, C.; Norden, B.; Rodger, A. *J. Am. Chem. Soc.* **1990**, *112*, 1971.
(35) Patel, K. K.; Plummer, E. A.; Darwish, M.; Rodger, A.; Hannon, M. J. *J. Inorg. Biochem.* **2002**, *91*, 220.
(36) Rodger, A.; Norden, B.; Rodger, P. M.; Bates, P. J. *Eur. J. Inorg. Chem.* **2002**, 49.
(37) Hard, T.; Norden, B. *Bioploymers* **1986**, *25*, 1209.
(38) Pasternack, R. F.; Giannetto, A. *J. Am. Chem. Soc.* **1991**, *113*, 7799.
(39) Hudson, B. P.; Sou, J.; Berger, D. J.; McMillin, D. R. *J. Am. Chem. Soc.* **1993**, *114*, 8997.
(40) Seifert, J. L.; Connor, R. E.; Kushon, S. A.; Wang, M.; Armitage, B. A. *J. Am. Chem. Soc.* **1999**, *121*, 2987.
(41) Marzilli, L. G.; Pettio, G.; Lin, M.; Kim, M. S.; Dixm, D. M. *J. Am. Chem. Soc.* **1992**, *114*, 7575.
(42) Chen, X.; Liu, M. *J. Inorg. Biochem.* **2003**, *94*, 106.
(43) Smith, J. O.; Olson, D. A.; Armitage, B. A. *J. Am. Chem. Soc.* **1999**, *121*, 2686.
(44) Wang, M.; Silva, G. L.; Armitage, B. A. *J. Am. Chem. Soc.* **2000**, *122*, 9977.
(45) *Circular Dichroism: Principles and Applications*; Berova, N., Nakanishi, K., Woody, R. W., Eds.; Wiley-VCH: New York, 2000.
Electronic excitation calculations using ZINDO and employing INDO/2 show that 5,6-dmp possesses higher dipolemoment, polarizability, and hyperpolarizability than the parent phen ligand. See Supporting Information, Table S7.

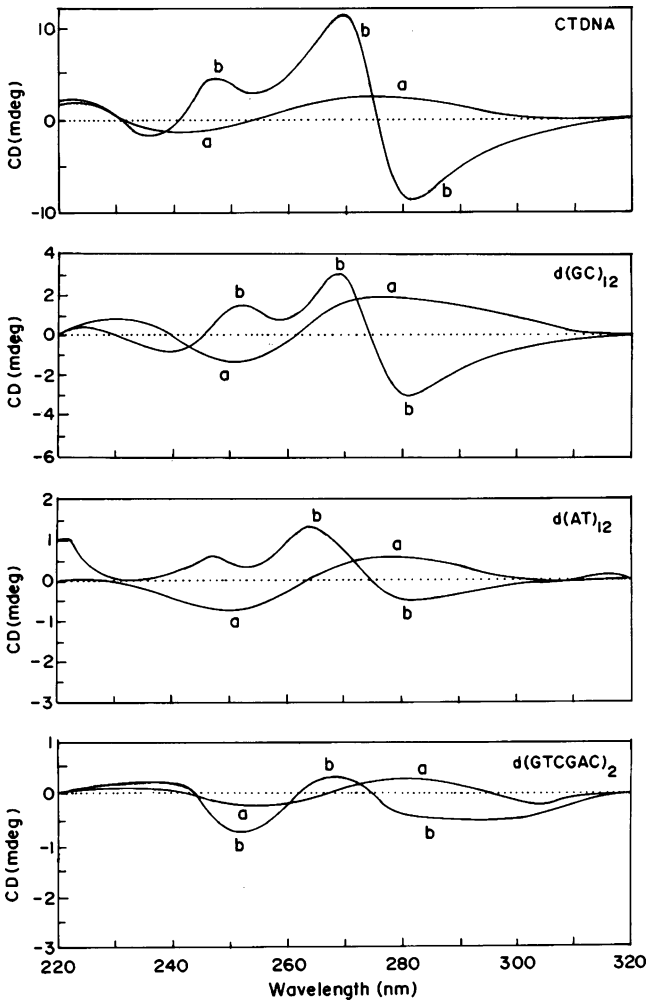

Figure 8. Circular dichroism spectra of CT DNA, d(AT)$_{12}$, d(GC)$_{12}$, and d(GTCGAC)$_2$ in the absence (a) and presence (b) of the *rac*-[Ru(5,6-dmp)$_3$]$^{2+}$ (concentration of the polynucleotides = 2×10^{-5} M; cell length = 0.2 cm).

When the 5,6-dmp complex is treated with polynucleotides, the exciton CD intensity decreases (Figure 8) in the order CT DNA ≫ poly d(GC)$_{12}$ > poly d(AT)$_{12}$ > d(GTCGAC)$_2$, which is consistent with the decreasing length of DNA and the preference of the complex to bind to GC rather than AT sequence. A similar observation has been made[46] for the dinuclear complex *rac*-[{Ru(5,6-dmp)$_2$}$_2$(μ-bpm)]$^{4+}$. The binding stoichiometries for the phen and 5,6-dmp complexes for interaction with the strongly binding poly d(GC)$_{12}$ with alternating guanine/cytosine sequence have been determined by the method of continuous variation. The method involves mixing of the ruthenium complex and the polynucleotide ([NP] concentration) in variable ratios but maintaining their total concentrations constant.[40] A plot of the CD intensity observed at 270 nm versus the mole fraction of the metal complex (X_{Ru}) exhibits an inflection, interestingly, at different X values of 0.25 and 0.65 respectively for phen and 5,6-dmp complexes, which correspond to binding stoichiometries (Figure 9). The inflections correspond to 1:2 Ru:NP or 1:1 Ru:base pair for the phen complex and 4:2

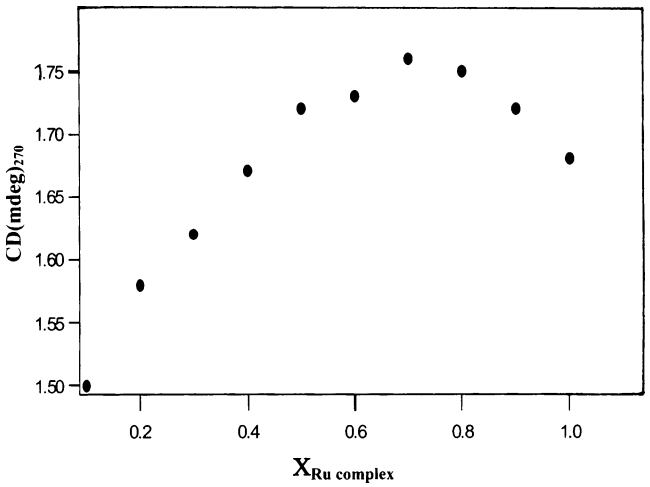

Figure 9. Job plot constructed from mixing *rac*-[Ru(5,6-dmp)$_3$]$^{2+}$ and poly d(GC)$_{12}$ together in variable ratios but at constant total concentration (2×10^{-5} M). CD intensities at 270 nm are plotted versus the mole fraction of the 5,6-dmp complex.

Ru:NP or 4:1 Ru:base pair for the 5,6-dmp complex. This reveals the formation on the duplex of high-nuclearity aggregates of the complex, that is 4 complex molecules to 1 base pair rather than 1 complex molecule to 1 base pair as for the phen analogue. Further, the 1:1 Ru:base pair stoichiometry observed for the phen complex could not be detected for the 5,6-dmp complex. However, an inflection at $1/R = 2$ (1 Ru/base pair) is observed in the CD spectra for the binding of the 5,6-dmp complex to CT DNA. The very high intensity of the exciton CD signal at $1/R$ values of 2 ($1/R$ = [Ru complex]/[NP]), that is at 2:1 Ru:DNA ratio, reveals the formation of a strong electronic and structural scaffold by the DNA-bound complex, which can couple with the unbound complex molecules.[41−44] A similar exciton coupling and helical aggregation of 6 rather than 4 molecules of *rac*-[Ru(5,6-dmp)$_2$(dppz)]$^{2+}$ bound preferentially to poly (AT)$_{12}$ rather than poly (GC)$_{12}$ has been observed.[23]

When the classical intercalator ethidium bromide (EthBr) is added to CT DNA ($R = 1$) incubated with *rac*-[Ru(5,6-dmp)$_3$]$^{2+}$ ($R = 2$), the exciton CD observed reverts back to a CD response typical of EthBr intercalated between the base pairs of the right-handed CT DNA. Also, when *rac*-[Ru(5,6-dmp)$_3$]$^{2+}$ is added to CT DNA ($R = 2$) incubated with EthBr ($R = 1$), a CD response typical of the classically intercalated EthBr is observed (Figure 10A,B). On the other hand, when *rac*-[Ru(phen)$_3$]$^{2+}$ is added to CT DNA ($R = 2$) incubated with *rac*-[Ru(5,6-dmp)$_3$]$^{2+}$ ($R = 2$) the exciton CD signal is not disturbed. Also, when *rac*-[Ru(5,6-dmp)$_3$]$^{2+}$ is added to CT DNA ($R = 2$) incubated with *rac*-[Ru(phen)$_3$]$^{2+}$ ($R = 2$), the CD pattern for the DNA binding of *rac*-[Ru(phen)$_3$]$^{2+}$ disappears and the biphasic CD signal is observed immediately (Figure 11A,B). All these observations reveal that the 5,6-dmp complex, which replaces a partial intercalator like [Ru(phen)$_3$]$^{2+}$ but not the classical intercalator EthBr, should involve stronger DNA binding.

Enantiopreferential DNA Dinding. Interestingly, the CD spectrum of the dialysate (Figure S7) obtained after dialysis of a solution of CT DNA (2.5 M) against a solution of *rac*-[Ru(5,6-dmp)$_3$]$^{2+}$ for 24 h at 4 °C is similar to that of free

(46) Uma Maheswari, P.; Rajendiran, V.; Palaniandavar, M. *Bull. Chem. Soc. Jpn.* **2005**, *78*, 835.

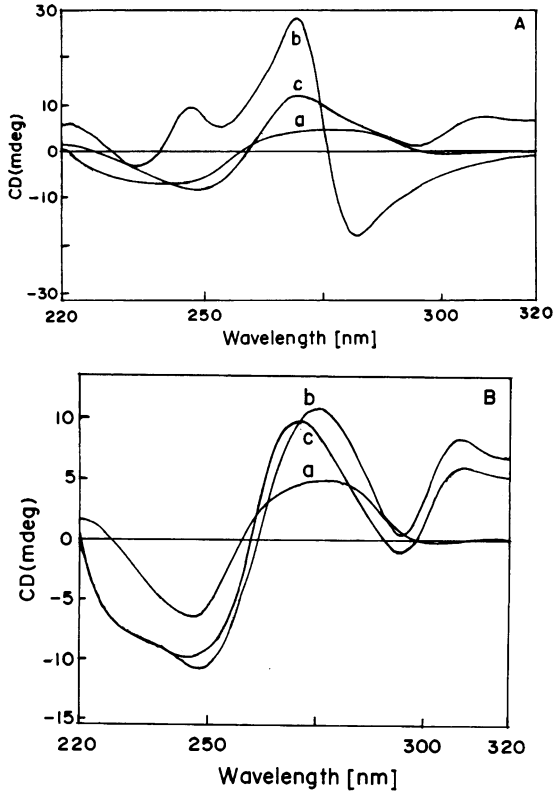

Figure 10. (A) Circular dichroism spectra of CT DNA in the absence (a) and presence (b) of *rac*-$[Ru(5,6\text{-dmp})_3]^{2+}$ at $1/R = 2$ and of CT DNA incubated with EthBr in the presence of *rac*-$[Ru(5,6\text{-dmp})_3]^{2+}$ at $1/R = 2$ (c) (concentration of CT DNA $= 2 \times 10^{-5}$ M). (B) Circular dichroism spectra of CT DNA in the absence (a) and presence (b) of EthBr at $1/R = 2$ and of CT DNA incubated with *rac*-$[Ru(5,6\text{-dmp})_3]^{2+}$ in the presence of EthBr at $1/R = 2$ (c) (concentration of CT DNA $= 2 \times 10^{-5}$ M).

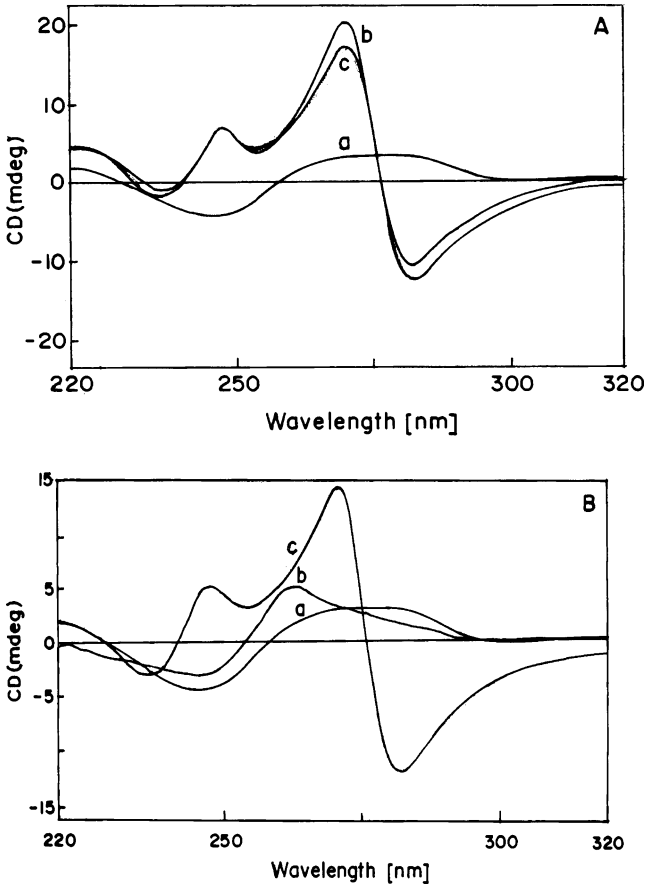

Figure 11. (A) Circular dichroism spectra of CT DNA in the absence (a) and presence (b) of *rac*-$[Ru(5,6\text{-dmp})_3]^{2+}$ at $1/R = 2$ and of CT DNA incubated with *rac*-$[Ru(phen)_3]^{2+}$ in the presence of *rac*-$[Ru(5,6\text{-dmp})_3]^{2+}$ at $1/R = 2$ (c) (concentration of CT DNA $= 2 \times 10^{-5}$ M). (B) Circular dichroism spectra of CT DNA in the absence (a) and presence (b) of *rac*-$[Ru(phen)_3]^{2+}$ at $1/R = 2$ and of CT DNA incubated with *rac*-$[Ru(5,6\text{-dmp})_3]^{2+}$ in the presence of *rac*-$[Ru(phen)_3]^{2+}$ at $1/R = 2$ (c) (concentration of CT DNA $= 2 \times 10^{-5}$ M).

Λ-enantiomer of $[Ru(5,6\text{-dmp})_3]^{2+}$ (tartrate salt)[44] suggesting the presence of Λ-$[Ru(5,6\text{-dmp})_3]^{2+}$ in the dialysate. Also, it is the inverse of that obtained for the addition of *rac*-complex to CT DNA, that is, for the preferential binding of Δ-enantiomer. This unambiquously reveals the preferential binding of Δ-enantiomer of the complex to the right-handed CT DNA. On increase of the ionic strength of a solution of the complex bound to CT DNA from 0 to 5 M NaCl, novel CD spectral features are observed.[44] At zero ionic strength a CD signal of high intensity typical of DNA-bound Δ-enantiomer is observed, and when it is increased from 0 to 0.2 M, the intensity decreased slowly (Figure 12A); on increase of it to 1.5 M NaCl, a disturbed CT DNA signal with decrease in intensity for both the positive and negative bands, but not exciton coupled CD, is observed. When it is further increased to 5 M NaCl, the CT DNA bands totally disappear and a CD signal exactly opposite to the exciton coupled CD signal observed at lower ionic strength, but with intensity less than the latter, is observed (Figures 12B and S8A). Both the CD signals possess the same crossover point but are exactly opposite in shape. This novel observation suggests that at lower ionic strength the Δ-enantiomer of the complex binds strongly to CT DNA, but at extremely higher ionic strengths the Λ-enantiomer binds but less strongly to CT DNA conformationally modified to Z-like form despite the lower GC content of the DNA. (Only poly $d(GC)_{12}$, the alternating polymer, is well-known to stabilize the Z conformation.) The difference in intensities of the CD signals obtained at low and high ionic strengths reveals that the exciton coupling of unbound Δ-enantiomer (bound to right-handed DNA) is stronger than that of Λ-enantiomer (bound to CT DNA possessing a Z-like distorted structure at higher ionic strengths) (Figure 13A). Similar observations were made (Figures 13B and S8B) when the experiment was carried out with poly $d(GC)_{12}$ at two extreme ionic strengths, confirming the enantiospecific binding and reversal of the *rac*-$[Ru(5,6\text{-dmp})_3]^{2+}$ depending upon the DNA conformation. This is in remarkable contrast to *rac*-$[Ru(5,6\text{-dmp})_2(dppz)]^{2+}$, which fails to show any reversal in enantiospecificity.[23] Strong partial intercalation of the dppz ligand stabilizes the B form of the DNA double helix from conversion to the Z form even at high ionic strength (5 M NaCl). Thus, all the above observations clearly reveal that the enantiopreferential binding of $[Ru(5,6\text{-dmp})_3]^{2+}$ is tuned to the DNA conformation, and similar observations have been made by Barton[18] for the DNA binding of $[Ru(4,7\text{-dip})_3]^{2+}$. The enantiopreferential DNA binding, which depends on the helicity of the chiral host, has also been observed[47] previously with certain types of porphyrins such as *trans*-bis(*N*-methylpyridinum-4-yl)diphenylporphyrin (*trans*-

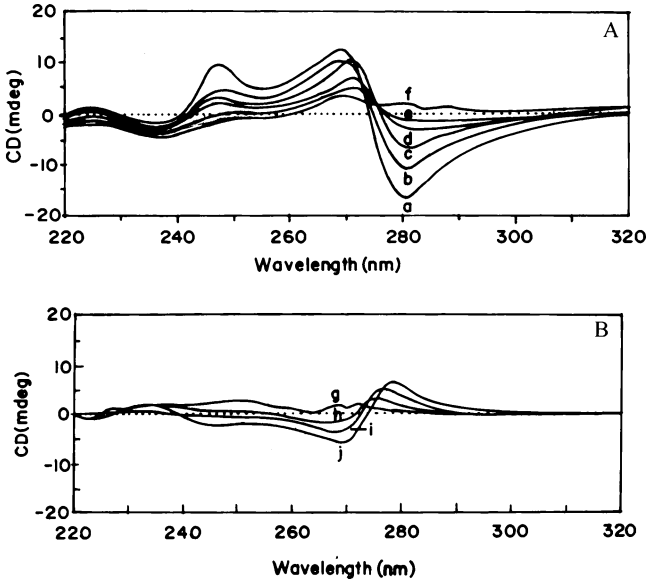

Figure 12. (A) Circular dichroism spectra of *rac*-[Ru(5,6-dmp)$_3$]$^{2+}$ at $1/R = 2$ in the presence of CT DNA, with varying NaCl concentration: 0 M (a); 0.05 M (b); 0.1 M (c); 0.15 M (d); 0.2 M (e); 0.25 M (f) (concentration of CT DNA $= 2 \times 10^{-5}$ M). (B) Circular dichroism spectra of *rac*-[Ru(5,6-dmp)$_3$]$^{2+}$ at $1/R = 2$ in the presence of CT DNA with varying NaCl concentration: 2.5 M (g); 3 M (h); 4 M (i); 5 M (j) (concentration of CT DNA $= 2 \times 10^{-5}$ M).

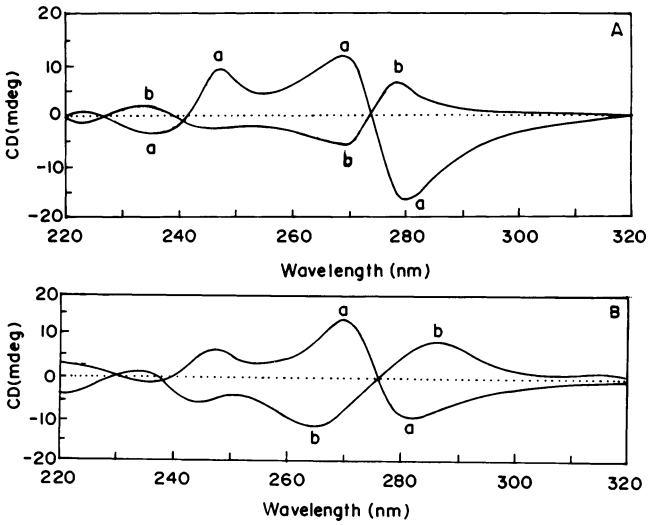

Figure 13. (A) Circular dichroism spectra of *rac*-[Ru(5,6-dmp)$_3$]$^{2+}$ ($1/R = 2$) in the presence of CT DNA, at 0.05 M (a) and 5 M NaCl (b) concentration (concentration of CT DNA $= 2 \times 10^{-5}$ M). (B) Circular dichroism spectra of *rac*-[Ru(5,6-dmp)$_3$]$^{2+}$ ($1/R = 2$) in the presence of poly d(GC)$_{12}$ at 0.05 M (a) and 5 M NaCl (b) concentration (concentration of DNA $= 2 \times 10^{-5}$ M).

H_2P_{agg}) on interaction with polypeptides of different helicities.

Thermal Denaturation Studies. The ΔT_m value for the interaction of [Ru(5,6-dmp)$_3$]$^{2+}$ with CT DNA for increasing $1/R$ (=[Ru complex]/[DNA]) values of 0.5, 1, and 1.5 increases as $7 < 12 < 17$, respectively. As the melting temperature of DNA (T_m) characterizes the transition from double-stranded to single-stranded DNA,[48] this observation suggests increased thermal stability of the duplex with increase in concentration of complex (Figure S9). Further, interestingly, the ΔT_m values range from that for a typical nonclassical intercalator to that for a strong metallointercalator, thus giving a clear indication about the strong binding of the complex. A similar increase in the ΔT_m values has been observed for the aggregation of certain cyanine dyes on PNA/DNA duplexes.[43]

Electrochemical Studies. The cyclic (CV) and differential pulse voltammetric (DPV) responses for the 5,6-dmp and phen complexes on an ITO electrode in Tris-HCl buffer in the presence and absence of CT DNA have been obtained and used to monitor the interaction with DNA (Table S6). The formal potential of the Ru(II)/Ru(III) couple ($E^{\circ\prime}$ or voltametric $E_{1/2}$) for the 5,6-dmp complex (1.033 V) is lower than its phen analogue (1.095 V), which is consistent with the stronger Ru−N bond evident from the X-ray structure of the complex. On the incremental addition of DNA to the metal complexes ($R = 0.25-4$), the peak currents of the anodic waves in the cyclic voltammograms of both the complexes become higher than those in the absence of DNA indicating that multiple turnovers of oxidation of DNA by the oxidized form of the metal complex occur during a single voltammetric sweep. At R values lower than 1, the catalytic currents observed for the 5,6-dmp complex are higher than those for phen analogue; this reveals that a larger number of complex molecules bound to DNA as aggregates (cf. above) are involved in the catalytic oxidation of guanine bases[49] of polymeric DNA. But at values beyond $R = 1$, the number of free complex molecules decreases due to increase in availability of DNA binding sites, and the catalytic current observed for phen complex becomes higher than that for the 5,6-dmp complex. This reveals that the phen complex, which partially inserts one of its phen rings, is efficient in metal ion-mediated oxidation of guanine more than the groove-bound 5,6-dmp complex. The differential pulse voltammograms of both the complexes in the absence and presence of CT DNA ($R = 4$) reveals that the drop in anodic peak current for the 5,6-dmp complex (60%) is much higher than that for the phen analogue (10%) (Figure 14A,B). This observation means that the 5,6-dmp complex is bound to DNA much more strongly than its phen analogue (cf. above), as the drop in anodic peak current is due to slower mass transfer of the DNA-bound complex to the surface of the electrode. Further, interestingly, on addition of DNA, the anodic peak potential of the 5,6-dmp complex becomes increasingly positive and then remains almost constant but that of the phen analogue remains almost constant beyond $R = 4$. Thus, on complex binding to DNA ($R = 4$), the $E_{1/2}$ of the 5,6-dmp complex becomes significantly more positive (104 mV) than that for the analogous phen complex (2 mV). This illustrates[50] that the 5,6-dmp complex is less efficient than the phen analogue in effecting metal ion-mediated oxidation of guanine of DNA. The DNA-bound 5,6-dmp complex is stabilized in Ru(II) rather than Ru(III) oxidation state obviously because the

(47) Pasternack, R. F.; Giannetto, A. *J. Am. Chem. Soc* **1991**, *113*, 7799.
(48) Nair, R. B.; Teng, E. S.; Kirkland, S. L.; Murphy C. J. *Inorg. Chem.* **1998**, *37*, 139.
(49) Yang, I. V.; Thorp, H. H. *J. Inorg. Chem.* **2000**, *39*, 4969.
(50) Johnston, D. H.; K. C. Glasgow, H. H. Thorp. *J. Am. Chem. Soc.* **1995**, *117*, 8933.

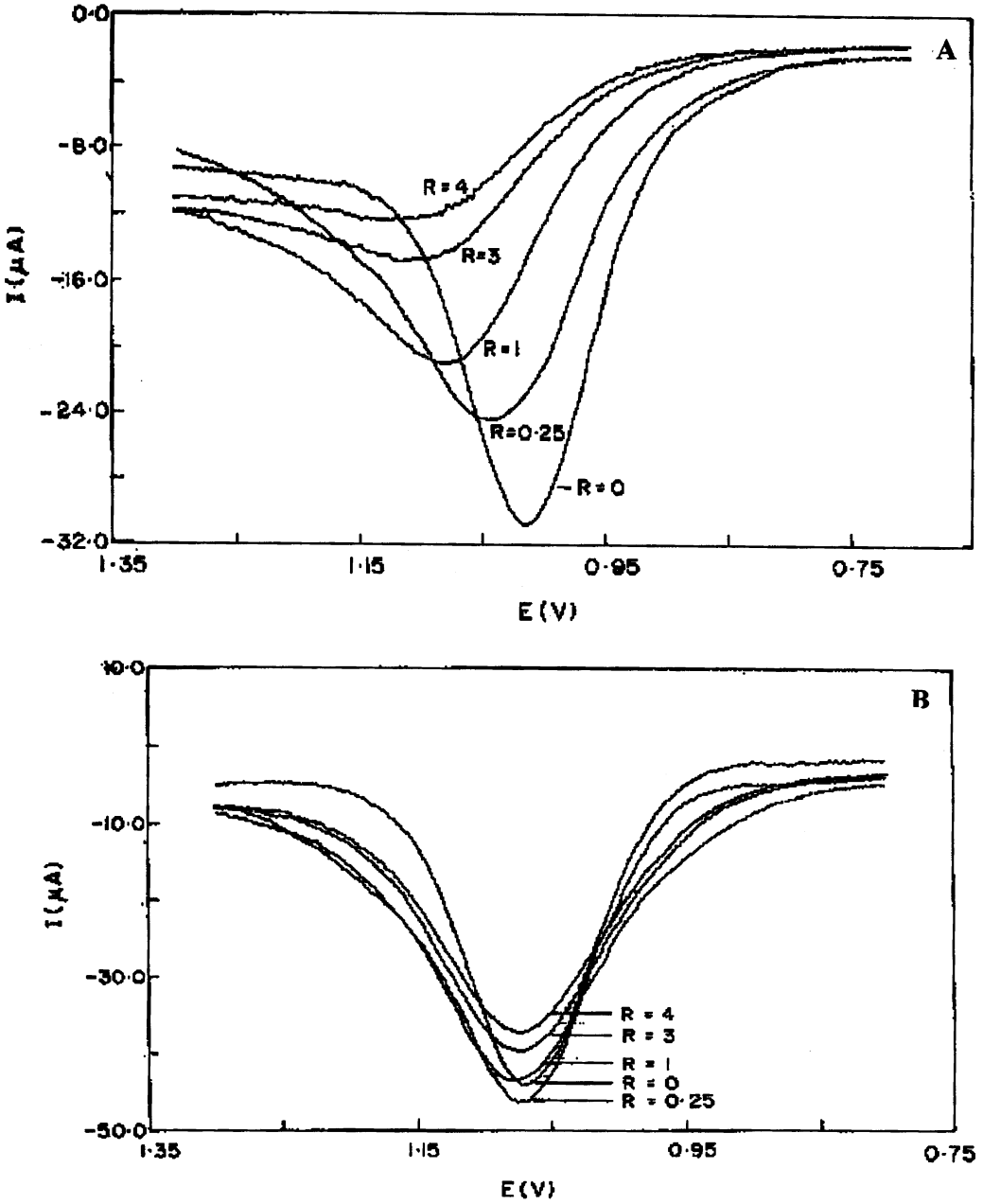

Figure 14. (A) Differential pulse voltammograms of 0.25 mM *rac*-$[Ru(5,6\text{-dmp})_3]^{2+}$ in the absence ($R = 0$) and presence ($R = 0.25-4$) of CT DNA (scan rate 5 mV s^{-1}; pulse height 50 mV; supporting electrolyte 50 mM NaCl). (B) Differential pulse voltammograms of 0.25 mM *rac*-$[Ru(phen)_3]^{2+}$ in the absence ($R = 0$) and presence ($R = 0.25-4$) of CT DNA (scan rate 5 mV s^{-1}; pulse height 50 mV; supporting electrolyte 50 mM NaCl).

hydrophobic interaction of the complex with DNA is facilitated in the lower oxidation state. Similar preferential stabilization of $[Ru(5,6\text{-dmp})_2(dppz)]^{2+}$ on DNA over its phen analogue in the lower Ru(II) oxidation state has been observed.[23] Thus, the significant changes in electrochemical parameters of the 5,6-dmp complex on DNA binding reveals the possibility of aggregation of the 5,6-dmp complex and further supports the above spectral results.

^{1}H NMR Studies. The ^{1}H NMR spectrum of poly $d(GC)_{12}$ was assigned (Figures S10A,B and S11) by carrying out two-dimensional NOESY and DQFCOSY experiments. The pattern of NOE's observed in the NOESY spectra is consistent with the oligonucleotide adopting a B-type DNA conformation in buffer solution. The identity of the aromatic protons (Figure 15A) of $[Ru(5,6\text{-dmp})_3]^{2+}$ in the presence of poly$(dGC)_{12}$ is confirmed by 2D DQF-COSY at 40 °C (Figure 16). Only one set of resonances is observed for $[Ru(5,6\text{-dmp})_3]^{2+}$ on interaction with the oligonucleotide at $1/R = 0.5$ (Figure 15C), indicating that the metal complex binds with fast exchange kinetics on the NMR time scale. It was noted, however, that the resonances from both $[Ru(5,6\text{-dmp})_3]^{2+}$ and the polynucleotide do exhibit high exchange broadening upon binding, particularly at low metal complex to oligonucleotide duplex ratios and at low temperatures (5−35 °C). Addition of the complex broadens the H8 and H6 protons of guanine/cytosine with small changes in chemical shifts but effects no changes in the hydrogen-bonded imino protons of the bases suggesting groove rather than intercalative DNA binding of the complex. On binding to DNA, the aromatic protons of $[Ru(5,6\text{-dmp})_3]^{2+}$ show large upfield

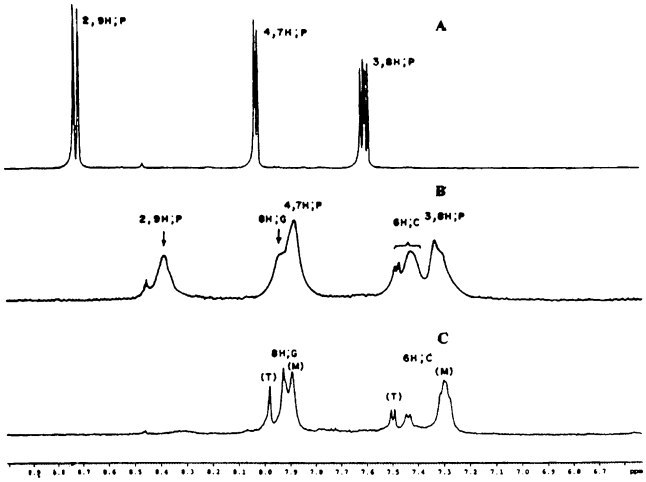

Figure 15. ^{1}H NMR spectra of the free complex *rac*-[Ru(5,6-dmp)$_3$]$^{2+}$ (A), complex + poly d(GC)$_{12}$ at 1/*R* of 0.5 (B), and free poly d(GC)$_{12}$ (C).

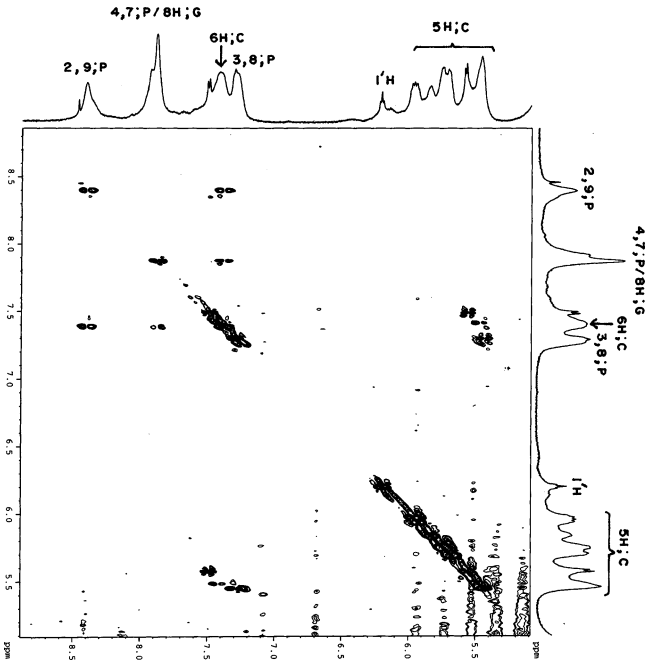

Figure 16. DQF-COSY spectrum of *rac*-[Ru(5,6-dmp)$_3$]$^{2+}$ interacted with poly d(GC)$_{12}$ at 1/*R* of 0.5 at 40 °C.

shifts on binding to poly(dGC)$_{12}$, varying in the following order: 2,9- (0.32 ppm) > 3,8- (0.28 ppm) > 4,7-protons (0.15 ppm). Also, the methyl protons of coordinated 5,6-dmp show an upfield shift of 0.37 ppm with high broadening revealing strong association of the ruthenium complex molecules on the oligonucleotide. The intermolecular contacts between DNA and metal complex were determined by running a NOESY spectrum at 40 °C (Figure 17). Strong NOE cross-peaks were observed between the three sets of aromatic protons of the ruthenium complex revealing a close association between the complex molecules in the presence of poly d(GC)$_{12}$, which is confirmed by the NOE peaks observed between the 5,6-methyl protons and the aromatic protons at the 2,9/3,8 and 4,7-positions of 5,6-dmp. Also, the NOE cross-peaks between protons of the complex and the sugar H1′and H3′ could not be observed. Also, the 2,9-protons show intense cross-peaks with the H2′, H2″ and very

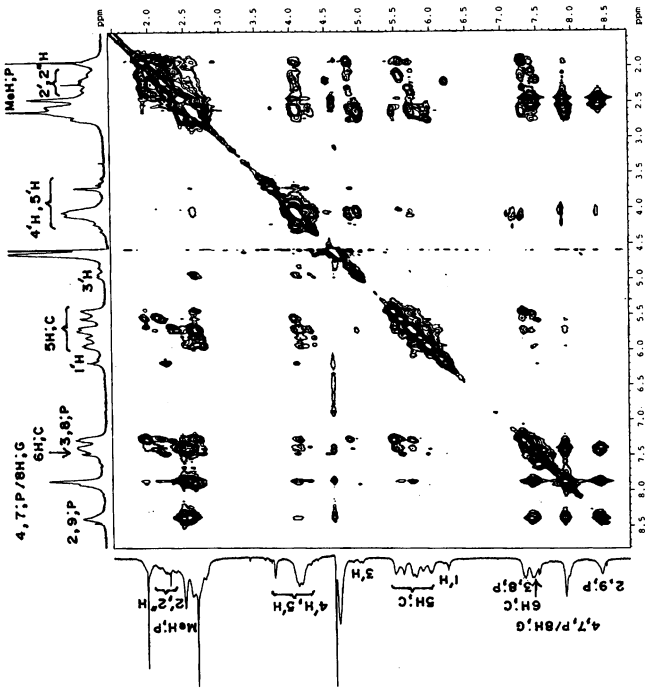

Figure 17. NOESY spectrum of *rac*-[Ru(5,6-dmp)$_3$]$^{2+}$ interacted with poly d(GC)$_{12}$ at 1/*R* of 0.5 at 40 °C.

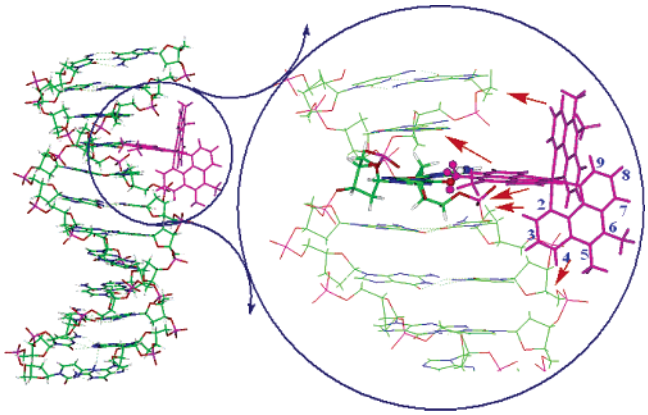

Figure 18. Molecular model constructed by using the constraints obtained from the ^{1}H, 2D NOESY NMR spectrum of [Ru(5,6-dmp)$_3$]$^{2+}$ bound to poly (GC)$_{12}$ in the major groove: an illustration showing the NOE interactions (indicated by red-colored arrows) observed in ^{1}H NMR between the sugar protons (2, 2″) and the 5,6-dmp complex (numbering scheme shown in blue) (generated and minimized using Insight II, Discover 3).

weak cross-peaks with the H4′, H5′ protons of poly d(GC)$_{12}$. As the former protons are only accessible from the major groove (Figure 18) and the latter from the minor groove, it is evident that the ruthenium complex binds mostly in the major rather than minor groove of the oligonucleotide. Attempts to study the interaction of [Ru(5,6-dmp)$_3$]$^{2+}$ with poly d(AT)$_{12}$ and poly d(GTCGAC)$_2$ failed due to higher broadening effects caused by intermediate exchange kinetics in the temperature range 5−45 °C.

Molecular Modeling. To obtain support for the DNA binding mode, the binding energies of the complex have been calculated with different sequences such as the Dickerson sequence d(GCGCATATGCGC)$_2$, poly d(GC)$_{12}$, and poly d(AT)$_{12}$. Initially, the complex was manually docked at different sites of DNA. Several starting geometries for

intermolecular complexes were selected by structure-based docking strategy and by considering all possible steric factors. After docking, minimizations were performed on the intermolecular complexes to remove short contacts and short molecular dynamics were made to generate a variety of starting geometries. A study on the interaction of various Cr(III) complexes with DNA has made it clear that the extensible systematic force field (ESFF) provides reliable estimates of binding energy and possible comparison with experimental results can be rationalized.[51,52] Different modes of binding with different starting geometries, including groove binding through major/minor groove, intercalation through major and minor groove, and simple electrostatic binding with any groove preference, were attempted with poly $d(GC)_{12}$, poly $d(AT)_{12}$, and the Dickerson sequence. It is found that binding of the 5,6-dmp complex in the major groove and to a lesser extent in the minor groove of poly $d(GC)_{12}$ is favored with no evidence for an intercalative mode of interaction (Figure S12). And for poly $d(AT)_{12}$ minor groove binding is favored much more than electrostatic and intercalative modes of binding. Interestingly, the complex is found to have better alignment on the GCGC end rather than on the central ATAT sequence of d(GCGCATATGCGC)$_2$. Also, specific groove binding of the complex is of little interest compared to an electrostatic mode of interaction through both the grooves.

DNA Binding Model. The strong binding of Δ-$[Ru(5,6\text{-}dmp)_3]^{2+}$ under racemic conditions to B-DNA and the resulting large induced CD are really intriguing despite the absence of partial intercalative mode of binding of the complex. Also, the possibility of "Pfeiffer CD"[53] is ruled out as Ru(II) complexes are substitution as well as inversion inert. Moreover, the ICD obtained immediately upon enantiopreferential binding of the complex is stable over time and at high temperatures, and thus there is no "diastereomeric equilibration" between the enantiomers. Spontaneous aggregation of $[Ru(5,6\text{-}dmp)_3]^{2+}$ molecules gives rise to large induced CD signals due to coupling of transition dipole moments of coordinated 5,6-dmp ligands, as they orient in an orderly manner on the grooves of DNA. But, though monodispersed at low ionic strength, the complex shows CD features consistent with the exciton coupling. Thus, the coordinated 5,6-dmp ligand with polarizability[45] (Table S7) higher than simple phen confers on the complex a tendency to aggregate on the DNA polymer, which is unique as analogous complexes of simple and other methyl-substituted phen ligands fail to show such a behavior. Also, the analogous $[Co(5,6\text{-}dmp)_3]^{2+}$ complex[54] with smaller size has been shown not to strongly bind to CT DNA, and no exciton coupling is observable. This illustrates the importance of size of the metal complex in enantiopreferential DNA binding. In fact, it is known that increased hydrophobicity of complexes enhances the DNA binding affinity and that an increase in steric bulk of the ligands leads to increased enantioselectivity.[8]

Conclusions

The complex cation *rac*-$[Ru(5,6\text{-}dmp)_3]^{2+}$ (5,6-dmp = 5,6-dimethyl-1,10-phenanthroline) possesses a distorted octahedral geometry in its X-ray crystal structure. The absorption, emission, and CD spectral and thermal denaturation studies suggest that hydrophobic interaction of coordinated 5,6-dmp ligand with DNA surface leads to strong DNA groove binding of the complex. Also, Ru(II) rather than Ru(III) form of the complex is stabilized on binding to DNA, which is also rendered stable toward electrocatalytic oxidation. Interestingly, the complex exhibits a remarkable enantiospecificity in DNA binding depending upon the conformation of DNA. Thus the Δ-enantiomer of the racemic complex preferentially binds to the right-handed B form of poly $d(GC)_{12}$ while the Λ-enantiomer binds to the Z form of poly $d(GC)_{12}$ generated from the B form by adding 5 M NaCl. The electrostatic binding mode of the complex on the DNA surface, conferred by 5,6-dimethyl substitution of phen ring, seems to provide a facile way of switching the enantiospecificity of the *rac*-complex with change in DNA conformation. This study illustrates how enantiospecificity in DNA binding is achieved by suitably tuning the phen ligand substituents. The observation of enantiospecificity would be helpful in designing specific chemical probes that can distinguish the handedness of DNA helices in solution.

Experimental Section

Materials and Methods. The self-complementary oligonucleotides d(GCGCGCGCGCGC) referred as $d(GC)_{12}$, d(ATATATATATAT) referred as $d(AT)_{12}$, and d(GTCGAC) referred as d(GTCGAC)$_2$ were purchased from The Microsynth GMB, Switzerland, and stored at −20 °C. The lyophilized oligonucleotides were digested in Tris buffer and annealed using standard procedures to make the double-stranded oligonucleotides and stored at 4 °C. The concentrations of the oligonucleotide solutions were determined spectrophotometrically using the molar absorptivities provided by the supplier: poly $d(GC)_{12}$, ϵ_{260nm} = 8550 M^{-1} (NP) cm^{-1}; poly $d(AT)_{12}$, ϵ_{260nm} = 10 892 M^{-1} (NP) cm^{-1}; d(GTCGAC)$_2$, ϵ_{260nm} = 9 330 M^{-1} (NP) cm^{-1}. $RuCl_3 \cdot 3H_2O$ was purchased from Arora Mathey Limited. 5,6-Dimethyl-1,10-phenanthroline, SP Sephadex C-25, sodium 4-toluenesulfonate, tetra-*n*-butylammonium chloride, and disodium dibenzoyltartrate (D,L) were purchased from Aldrich Chemicals. The disodium salt of calf thymus DNA (highly polymerized) purchased from Sigma was stored at 4 °C and used as received. Ultrapure Milli Q water (18.2 mΩ) was used in all experiments. Solutions of DNA in buffer, 50 mM NaCl/5 mM Tris HCl in water, gave the ratio of UV absorbance at 260 and 280 nm, A_{260}/A_{280}, of 1.9, indicating that the DNA was sufficiently free of protein.[26] Concentrated stock solutions of DNA (10.5 mM) were prepared in buffer and sonicated for 25 cycles, where each cycle consisted of 30 s with 1 min intervals. The concentration of DNA in nucleotide phosphate (NP) was determined by UV absorbance at 260 nm after 1:100 dilutions. The extinction coefficient, ϵ_{260}, was taken as 6600 M^{-1} cm^{-1}. Stock solutions were stored at 4 °C and used after no more than 4 days. The complex *rac*-$[Ru(phen)_3]Cl_2$ was prepared and purified as reported earlier (λ_{max}, 440 nm; ϵ, 20 000 M^{-1} cm^{-1} in H_2O).[14]

(51) Shi, S.; Yan, L.; Fisher, J. *ESFF Force field Project Report II*; MSI: San Diego, CA.
(52) Vijayalakshmi, R.; Subramanian, V.; Unni Nair, B. *J. Biomol. Struct. Dyn.* **2002**, *19*, 1.
(53) Pfeifer, P.; Nakatsuka, Y. *Ber. Dtsch. Chem. Ges.* **1933**, *66B*, 415.
(54) Tamilselvi, P.; Palaniandavar, M. *Inorg. Chim. Acta* **2002**, *337*, 420.

Synthesis of Δ-, Λ-, and *rac*-[Ru(5,6-dmp)$_3$]$^{2+}$. *rac*-[Ru(5,6-dmp)$_3$]$^{2+}$ was synthesized using the procedure reported for [Ru(phen)$_3$]$^{2+}$.[29] The product was isolated as the PF_6^- salt and then converted into its chloride by treating it with tetra-*n*-butylammonium chloride in acetone solution. The product was purified using SP-sephadex C-25, the Δ-enantiomer was separated on a Sephadex SP-C 25 column (40 × 2.5 cm) using 0.1 M disodium dibenzoyl-L-tartrate, 0.2 M sodium chloride, and 20% acetone as the eluent, and the Λ-enantiomer was separated using a procedure similar to that above but using disodium dibenzoyl-D-tartrate as eluent. The enantiomeric purity of the tartrate salt was assayed by CD spectroscopy. UV−visible for *rac*-[Ru(5,6-dmp)$_3$]$^{2+}$: λ_{max} nm (ϵ_{max}) 455 (19 500), 430 (18 200), 270 (1 00 000), 242 (65 900). ^{1}H NMR (D_2O): δ 8.7 (d), 8.02 (d), 7.6 (q), 2.84 (s). Δ-enantiomer (CD signals): +247, +270, −280, +430, −502 nm. Λ-enantiomer (CD signals): −247, −270, +280, −430, +502 nm. Both the enantiomers have zero crossovers at 275 and 452 nm. Attempts to separate the chloride salt into enantiomerically pure Δ- and Λ-enantiomers were not fruitful.

Crystallography. Single crystals of the complex were grown from an aqueous Tris-HCl buffer solution by slow evaporation. Significant crystal data and data collection parameters are listed in Table S1. The intensity data were collected at 173 K (−100 °C) on a Stoe Mark II-image plate diffraction system[55] equipped with a two-circle goniometer and using Mo Kα graphite-monochromated radiation: image plate distance 100 mm; ω rotation scans 0−180° at ϕ 0° and 0−20° at ϕ 90°; step $\Delta\omega = 1.5°$; exposure 2 min/image; 2θ range 2.29−59.53°; $d_{min} - d_{max} = 17.779-0.716$ Å. The structure was solved by direct methods using the program SHELXS-97.[56] The refinement and all further calculations were carried out using SHELXL-97.[57] The H atoms were included in calculated positions and treated as riding atoms using SHELXL default parameters. The non-H atoms were refined anisotropically, using weighted full-matrix least squares on F^2. No absorption correction was applied. Two Cl^- anions are present with one disordered over two sites (occupancies 0.5/0.5). A total of 13 water molecules of crystallization could be located, with one disordered over two sites (occupancies 0.5/0.5). It was not possible to locate the water H atoms. Perspective views of the molecules are obtained by PLATON.[58]

Absorption Spectral Studies. Absorption spectra were recorded on a Varian Cary (300) Bio UV−vis spectrophotomer using cuvettes of 1 cm path length. For UV−vis spectral titrations 4×10^{-5} M concentration of ruthenium solutions were used and calf thymus DNA was added in steps until $R = 40$. Intense MLCT bands were monitored to follow the interaction of the complexes with CT DNA. All the titrations were done using DNA stock solutions pretreated with the metal complex to take care of the dilution effects. Fits of experimental absorption titrations were performed with Mathematica v3.

Steady-State and Time-Resolved Luminescence Spectral Studies. Emission intensity measurements were carried out by using a Hitachi F 4500 spectrofluorometer. Tris buffer was used as a blank to make preliminary adjustments. The excitation wavelength was fixed, and the emission range was adjusted before measurements. All measurements were made at 25 °C in a thermostated cuvette holder with 5 nm entrance slit and 5 nm exit slit. For emission spectral titrations 10×10^{-6} M concentration of ruthenium solutions were used and calf thymus DNA was added in steps until $R = 10$. The emission enhancement factors were measured by comparing the intensities at the emission spectral maxima in the absence and presence of DNA, under similar conditions. Temperature variation emission measurements were done using an externally fitted Peltier setup using a 1 cm quartz cuvette.

The fluorescence decay measurements of the DNA bound complexes were carried out using the time-correlated single photon counting technique (TCSPC) by exciting the sample at 455 nm (model 5000U, LED, IBH, U.K.) with a micro channel plate photomultiplier tube (MCP-PMT) as detector. Temperature variation was done using a water-circulated thermostat. The measured fluorescence decay is the convolution true fluorescence decay with excitation function and instrument response function. The data analysis was carried out by the software provided by IBH (DAS-6), which is based on a reconvolution technique using iterative nonlinear least-squares methods. The reconvolution is preceded by a series of iterations untill χ^2 is reduced. The quality of fit is normally identified by the reduced χ^2, weighted residual, and the autocorrelation function of the residuals.

Circular Dichroic Spectral Studies. Circular dichroic spectra of DNA were obtained by using JASCO J-716 spectropolarimeter equipped with a peltier temperature control device. All experiments were done using a 1 or 0.2 cm path quartz cell. Each CD spectrum was collected after averaging over at least 4 accumulations using a scan speed of 100 nm min^{-1} and a 1 s response time. Machine plus cuvette baselines were subtracted and the resultant spectra zeroed outside the absorption bands. For temperature variation experiments, a temperature wavelength scan measurement was used to collect the spectra. The sample was typically heated from 7 to 87 °C at a ramp rate of 40 °C h^{-1} and a CD spectrum collected every 10 °C. No equilibration time was allowed prior to the collection of the spectrum. Equilibrium dialysis experiments were done using dialysis tube of 12 000 KD. A 2 mL sample of calf thymus DNA was dialyzed against 80 mL of buffer containing ruthenium complex, and solutions were dialyzed for 48 h with continuous agitation at 4 °C.

Thermal Denaturation Studies. DNA melting experiments were carried out by monitoring the absorption (260 nm) of CT DNA (160 μM) at various temperatures, in the absence and in the presence ($1/R = 0.5, 1.0, 1.5$) of the complex. The differences in the melting temperatures (ΔT_m range between which 10% and 90% of the absorption increase occurred) were then calculated.

NMR Spectroscopy. ^{1}H NMR spectra were recorded on a Bruker 500 MHz spectrometer. NOESY spectra were recorded by the method of States et al. using 2048 data points in t_2 for 256 t_1 values with a pulse repetition delay of 2 s. DQF-COSY experiments were accumulated using 2048 data points in t_2 for 256 t_1 values with a pulse repetition delay of 2 s. Spectra recorded in 90% H_2O and 10% D_2O were collected using the WATER GATE solvent suppression technique of Piotto et al. ^{1}H chemical shifts are relative to (tetramethylsilyl)propionic acid (TSP) as internal standard. Typical samples contained 1 mM poly d(GC)$_{12}$ duplex, 0.75 mM ruthenium complex, 20 mM NaCl, and 1 mM sodium cacodylate buffer (pH 7) in 0.5 mL of D_2O.

Electrochemistry. All the cyclic (CV) and differential pulse voltammetry (DPV) experiments were performed in a single compartment cell with a three-electrode configuration on an EG&G PAR 273 potentiostat/galvanostat equipped with P IV computer. Tin-doped indium oxide (ITO) was the working electrode, and the reference was a saturated calomel electrode. A platinum plate was

(55) *X-Area V1.17 & X-RED32 V1.04 Software*; Stoe & Cie GmbH: Darmstadt, Germany, 2002.
(56) Sheldrick, G. M. SHELXS-97 Program for Crystal Structure Determination. *Acta Crystallogr.* **1990**, *A46*, 467.
(57) Sheldrick, G. *SHELXL-97*; Universität Göttingen: Göttingen, Germany, 1999.
(58) Spek, A. L. *J. Appl. Crystallogr.* **2003**, *36*, 7.

used as the counter electrode. The supporting electrolyte was 50 mM NaCl/5 mM Tris HCl buffer at pH 7.1. Solutions were deoxygenated by purging with argon gas for 15 min prior to the measurements, and during the measurements a stream of argon was passed over the solution. All measurements were carried out at 25.0 ± 0.2 °C, maintained by a Haake D8-G circulating bath. The redox potential $E_{1/2}$ was calculated from the anodic (E_{pa}) and cathodic (E_{pc}) peak potentials of CV traces as $(E_{pa} + E_{pc})/2$ and also from the peak potential (E_{pa}) of DPV response as $E_p + \Delta E/2$ (ΔE is the pulse height).

Molecular Modeling. Molecular modeling was performed on a Silicon Graphics O2 workstation using the Biosym Modeling package from Molecular Simulation Inc. (San Diego, CA). The B-DNA systems chosen for the study were the dodecamer duplex of sequences $d(AT)_{12}$, $d(CGCGAATTCGCG)_2$, and $d(GC)_{12}$. Models of 12-mer nucleotides were constructed using the Biopolymer program of the Insight II package. The ruthenium complexes chosen for the molecular mechanical studies with DNA were constructed using the coordinates from the crystal strucutres and/or Insight II library. The metal complexes and each metal/DNA complex were subjected for minimization using the extensible systematic force field (ESFF)[51] with a nonbonded cutoff of 10 Å and a sigmoidal distant-dependent dielectric function ($\epsilon = 4r_{ij}$), which has been demonstrated to be an appropriate implicit treatment for the dielectric function in computing the electrostatic potential of nucleic acid. The energy minimization employed a steepest descent followed by conjugate gradient algorithms until the convergence criterion was reached. The geometry of the whole complex was then refined until convergence (criterion of root mean square (rms) energy gradient of 0.05 kcal/mol Å) was reached through out. Interaction energies of Ru−DNA complexes can be estimated by calculating the difference between their total energies and the sum of lowest energies found for the optimized structures of free DNA and binuclear complex. The negative of the interaction energy is the binding energy,

$$\text{IE} = \text{TE} - \text{sum of the individual energy} = -\text{IE} = \text{BE}$$

where, IE is the interaction energy, TE is the total energy of DNA/complex, and BE is the binding energy.[51]

Acknowledgment. The authors thank the Council of Scientific and Industrial Research, New Delhi, India, for financial support (Grant No. 01(1693)/01/EMR-II), Department of Atomic Energy, Mumbai, India (Grant No. 2003/37/25/BRNS), and a Senior Research Fellowship to P.U.M. The Chairman, Molecular Biophysics Unit, Indian Institute of Science, Bangalore, India, is gratefully acknowledged for use of the Circular Dichroism Spectral facility. Professor P. Natarajan and Dr. P. Ramamurthy, National Center for Ultra Fast Processes, are thanked for the lifetime measurements. Dr. V. Subramanian and R. Parthasarathi, Central Leather Research Institute, Chennai, India, are thanked for the molecular modeling studies. The UV−vis and fluorescence spectral facilities in the Department were created by funding respectively from the Department of Science and Technology (DST-FIST) and University Grants Commision (SAP I), New Delhi.

Supporting Information Available: X-ray crystallographic data for *rac*-$[Ru(5,6\text{-dmp})_3]^{2+}$ (Tables S1−S5), X-ray crystallographic files (CIF), electrochemical data for *rac*-$[Ru(5,6\text{-dmp})_3]^{2+}$ and *rac*-$[Ru(phen)_3]^{2+}$ (Table S6), polarizability data for *rac*-$[Ru(5,6\text{-dmp})_3]^{2+}$ (Table S7), and circular dichroism, thermal denaturation, NMR, and molecular modeling data (Figures S1−S12). This material is available free of charge via the Internet at http://pubs.acs.org.

IC050940Q